

## Research Article

# Coupled THM and Matrix Stability Modeling of Hydroshearing Stimulation in a Coupled Fracture-Matrix Hot Volcanic System

Yong Xiao <sup>1,2</sup> Jianchun Guo <sup>2</sup> Hehua Wang,<sup>1,3</sup> Lize Lu,<sup>1,3</sup>  
John McLennan,<sup>4</sup> and Mengting Chen<sup>5</sup>

<sup>1</sup>China Zhenhua Oil Co., Ltd, Beijing, China

<sup>2</sup>State Key Laboratory on Oil and Gas Reservoir Geology and Exploitation, Southwest Petroleum University, Chengdu, China

<sup>3</sup>Chengdu Northern Petroleum Exploration and Development Technology Co., Ltd., Chengdu, Sichuan, China

<sup>4</sup>Energy & Geoscience Institute, University of Utah, UT, USA

<sup>5</sup>Borehole Operation Branch Office of Sinopec Southwest Petroleum Engineering Co., Ltd., Sichuan, China

Correspondence should be addressed to Jianchun Guo; guojianchun@vip.163.com

Received 20 March 2018; Accepted 30 May 2018; Published 3 July 2018

Academic Editor: Mohammed Nouari

Copyright © 2018 Yong Xiao et al. This is an open access article distributed under the Creative Commons Attribution License, which permits unrestricted use, distribution, and reproduction in any medium, provided the original work is properly cited.

A coupled thermal-hydraulic-mechanical (THM) model is developed to simulate the combined effect of fracture fluid flow, heat transfer from the matrix to injected fluid, and shearing dilation behaviors in a coupled fracture-matrix hot volcanic reservoir system. Fluid flows in the fracture are calculated based on the cubic law. Heat transfer within the fracture involved is thermal conduction, thermal advection, and thermal dispersion; within the reservoir matrix, thermal conduction is the only mode of heat transfer. In view of the expansion of the fracture network, deformation and thermal-induced stress model are added to the matrix node's in situ stress environment in each time step to analyze the stability of the matrix. A series of results from the coupled THM model, induced stress, and matrix stability indicate that thermal-induced aperture plays a dominant role near the injection well to enhance the conductivity of the fracture. Away from the injection well, the conductivity of the fracture is contributed by shear dilation. The induced stress has the maximum value at the injection point; the deformation-induced stress has large value with smaller affected range; on the contrary, thermal-induced stress has small value with larger affected range. Matrix stability simulation results indicate that the stability of the matrix nodes may be destroyed; this mechanism is helpful to create complex fracture networks.

## 1. Introduction

With the increase of energy consumption, the exploration and development of oil and gas has gradually shifted from the conventional to unconventional reservoir, such as volcanic reservoirs [1, 2]. The volcanic reservoir has the characteristics of high temperature gradient and rock mechanical strength, and natural fractures are an important indicator of economic viability. The most important consideration for oil and gas or geothermal energy development in volcanic reservoirs is the use of hydraulic stimulation technology to establish a fracture network to effectively conduct fluid between injection and production wells [3–7]. In hydraulic fracturing associated with oil & gas or enhanced geothermal energy extraction, significant differences in surface pumping pressure and the injectivity index are common, even in the same field, as shown in Table 1.

The purpose of fracturing is to improve the conductivity of natural fractures and possibly extend or develop new fractures [4–8]. As Table 1 indicates, hydraulic fracturing can include extreme (high or low) injection pressure and often there are relatively low injection rates with large total injected volumes. Researchers [9, 10] found that two factors contributed to the difficulty of hydraulic stimulation: (1) with the propensity for reactivation of existing faults, and extension or shearing of natural fractures, hydraulic stimulation in volcanic reservoirs is sometimes referred to as hydroshearing; (2) these stimulation behaviors encompassed in thermal-hydraulic-mechanical (THM) or thermal-hydraulic-chemical (THC), such as shear dilation and thermomechanical aperture closure.

The injected water flow pattern of the volcanic reservoir is mainly controlled by the network of preexisting and induced

TABLE 1: Injectivity index during stimulations in hydrocarbon and geothermal granitic formations.

Different Energy Development	Project	Depth m	Lithology	Max. Inj. Rate m <sup>3</sup> /min	Inj. Pressure MPa/m	Total Injection Volume m <sup>3</sup>	Injectivity Indices kg/sec/MPa	Reference
Oil and Gas	Liaohe: #1	3022		6.4	0.0218	572	1.62	/
	Liaohe: #2	4772	Granite	5.5	0.0145	498	1.33	/
	Liaohe: #3	4188	Gneiss	4.4	0.0205	480	0.85	/
Geothermal	GPK2	3600	Granite	3.6	0.0036	30000	4.62	(Baria, 2009)
	Habanero 1	4421	Granite	1.8	0.0147	20000	1.00	[21]
	Habanero 4	4205	Granite	3.2	0.0114	27000	16.00	[21]
	RRG-9 ST-1	1524	Granite	1.0	0.0036	/	3.03	[22]

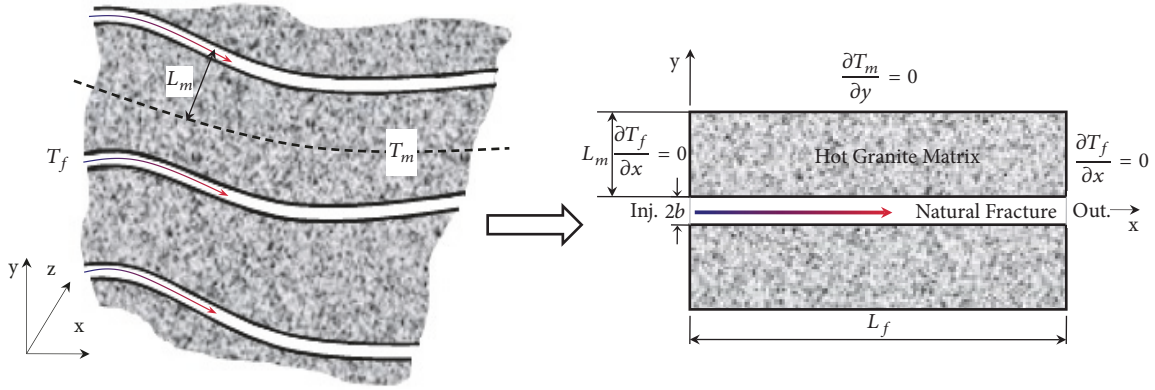


FIGURE 1: Idealized hot matrix-natural fracture system.

natural fractures and is affected by changes in conductivity resulting from heat transfer, shear dilation, and chemical processes. Many detailed studies of the precipitation/dissolution processes and their impact on fracture aperture variation in fractured volcanic reservoirs can be found in the literature [11–13]. The results show, in short-term hydroshearing fracturing, the effect of chemical action on the aperture change is smaller than thermal and mechanical processes, so it can be neglected. Therefore, when employing hydroshearing in the volcanic reservoir, aperture changes due to shear dilation and thermal stress result in the decrease of net pressure and growth of contract area between fracture planes, and this in turn affects fluid flows, heat transfer, and shear behaviors [14, 15]. To explain these behaviors, the authors built a modeling structure that couples thermal, hydraulic, and mechanical effects (THM) and apply this simulator to a hot granite reservoir to examine the importance of this coupling.

Because of the complexities of the numerical modeling, deformation and thermal-induced stress are often neglected and the matrix nodes assume stability and no secondary fractures form [16]. This paper describes a displacement discontinuity method [17] to solve the deformation-induced stress. The fracture is considered as a displacement discontinuity over a finite-length segment, which is treated as the inner boundary condition of the problem [18, 19]. After the given induced stress, the new stress state of the matrix nodes can be updated. The new stress state consists of three parts: initial stress, deformation-induced stress, and thermal-induced stress. The new stress state will affect the stability of the rock matrix and help to create complex fracture networks.

## 2. Physical System and Governing Equations

The hot and fractured volcanic oil & gas reservoir is always considered nonpermeability, and natural fractures within the matrix are the channels for fluid flow and heat exchange. Based on the simple principle of reducing the extremely complex system to an idealized one, an idealized system for integrating hot matrix and natural fracture is established to study the fracture deformation and their induced stress. The geometry of the conceptually idealized model corresponding to a fracture-matrix coupled system is shown in Figure 1.

The upstream boundary along the fracture axis represents the injection well (inlet), and the downstream boundary is the production well (outlet).

### 2.1. Fracture Fluid Flow Model and Heat Transfer

**2.1.1. Fracture Fluid Flow Model.** It is assumed that the fracture aperture varies in space and time, and the interface of the fracture does not leak-off so fluid flows along the natural fracture. The fracture is assumed to correspond to a parallel-plate system, and the laminar flow is valid. Without considering the slip effect, the velocity is integrated in the fracture cross section [20]. For this fracture system, the momentum balance indicates that the average flow velocity per unit length is proportional to the pressure gradient. The fracture fluid flow model is

$$u_x(x, t) = \frac{w^2(x, t)}{12\mu} \left( -\frac{\partial P(x, 0, t)}{\partial x} \right) \quad (1)$$

where  $u$  is the average velocity in the fracture per unit length,  $w$  is the average aperture or width of the fracture unit length,  $\mu$  is the viscosity of the injected fluid which is assumed to be a static value,  $P(x, 0, t)$  is the fluid pressure within the fracture ( $y=0$ ),  $x$  is the position, and  $t$  is the time. Assuming that there is no leak-off and the injected fluid is incompressible, according to the continuity equation, fluid discharge and changes per unit height can be written as

$$\begin{aligned} q(x, t) &= w(x, t) u_x(x, t) \\ \frac{\partial q(x, t)}{\partial x} &= 0 \end{aligned} \quad (2)$$

where  $q(x, t)$  is the volume flow. The fracture deformation and heat transfer are based on the balance of energy and mass, respectively. The flow equations will be coupled with the fracture constitutive model and thermal-induced aperture change model.

**2.1.2. Heat Transfer Equations.** Temperature differences drive the heat transfer between the hot reservoir matrix and injected cold water. The main mechanisms involved are thermal conduction, thermal advection, and thermal dispersion

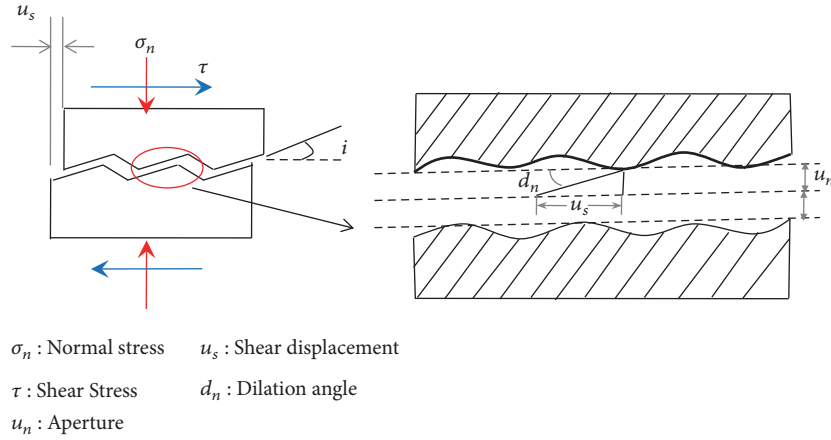


FIGURE 2: Graphs of the fracture aperture caused by shear displacement and dilation.

within the fracture, conduction-limited thermal transport from the reservoir matrix to the fracture. Within the reservoir matrix, thermal conduction is the only mode of heat transfer [20].

The following general assumptions are used in this simulation for calculating the fracture's temperature profile in each time step: (1) specific heat capacities of the matrix and injected water are not functions of temperature (in other words, they are static parameters); (2) there is no fluid leak-off from the interface into rock matrix (i.e., pressure equilibrium exists between the fracture and the reservoir matrix). The governing equations used in this fracture and the reservoir matrix heat transfer studies are given as

$$\rho_f c_f \frac{\partial \vec{T}_f}{\partial t} = -\rho_f c_f \vec{u} \nabla \vec{T}_f + K_{f,eff} \nabla^2 \vec{T}_f + \alpha_f h_{mf} \nabla \vec{T}_m \Big|_{y=b} \quad (3)$$

$$\rho_s c_s \frac{\partial \vec{T}_m}{\partial t} = K_{m,eff} \nabla^2 \vec{T}_m - \alpha_f h_{mf} \nabla \vec{T}_m \Big|_{y=b}$$

where  $t$  is the time;  $T_m$  and  $T_f$  are temperature in the matrix and fracture, separately;  $\rho_s$  and  $\rho_f$  are rock and water density;  $c_s$  and  $c_f$  are rock and water heat capacity;  $K_{m,eff}$  is the rock thermal conductivity.

## 2.2. Fracture Constitutive Model and Deformation-Induced Stress

**2.2.1. Fracture Constitutive Model.** The rough surface of a natural fracture is always undulating. During the hydroshearing stimulation, the effective normal stress of the fracture surface will continue to decrease, and the permanent shear displacement will be generated. The interface of the natural fracture will no longer completely overlap under normal stress and the dilation aperture  $u_d$  will increase because of shear displacement, as shown in Figure 2.

In 1985, Barton [23] summarized a nonlinear peak shear strength equation that was based on the joint surface

roughness coefficient and the compressive strength (as represented by JRC and JCS):

$$\tau = \sigma_n \tan \left[ \phi_r + JRC \log_{10} \left( \frac{JCS}{\sigma_n} \right) \right] \quad (4)$$

where  $\phi_r$  is the internal friction angle, the angle within the brackets is called the friction angle or residual friction angle. The latter term  $JRC \log_{10} (JCS/\sigma_n)$  is called the dilation angle which is closely related to the normal aperture of the fracture surface. The simplest relation between shear strain and stress before peak strength can be described in a linear equation as

$$\tau = k_s u_s \quad 0 \leq u_s \leq u_s^p \quad (5)$$

$$k_s = \frac{\sigma_n \tan [\phi_r + JRC_n \log_{10} (JCS_n/\sigma_n)]}{(L_n/500) [JRC_n/L_n]^{0.33}} \quad 0 \leq u_s \leq u_s^p \quad (6)$$

where  $k_s$  is the shear stiffness,  $u_s^p$  is shear displacement at peak strength, and  $L_n$  is the length of the fracture sample. Dilation is defined as a function of shear displacement and tangent of the dynamic dilation angle; the equation is shown as

$$du_n = \tan(d_n) du_s = \tan(d_n) \frac{1}{k_s} d\tau \quad (7)$$

where  $d_n$  is the dynamic dilation angle. Barton and Choubey [24] estimated the value of the mobilized dilation using the following empirically derived equation.

$$d_{n-dynamic} = \frac{1}{2JRC_{n-dynamic} \log_{10} (JCS_n/\sigma'_n)} \quad (8)$$

**2.2.2. Deformation-Induced Stress.** The elastic displacement discontinuity method (DDM) is an indirect boundary element method to cope those problems involving pure elastic nonporous media containing discontinuous surfaces or thin fractures [17]. The elastic DDM is based on analytical solution for the infinite two-dimensional homogeneous and

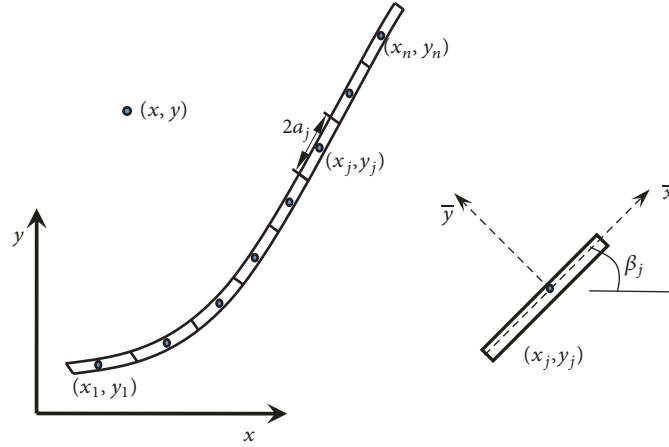


FIGURE 3: The local coordinate distribution after the discretization of natural fracture boundary.

isotropic elastic nonporous medium containing a finite small thin fracture with constant normal and shear displacement discontinuities. For an infinite elastic nonporous medium, the fractures are divided into  $N$  elemental segments with the displacement in each segment assumed to have a constant discontinuity. At any point  $(x, y)$ , the influence of displacement discontinuities from all fractures in the system can be obtained by summing the effects of all  $N$  elements using the fundamental analytical solutions. The fracture length is  $2a$  ( $a$  is the half length of fracture segment) and its center is located at  $(0, 0)$  as shown in Figure 3.

The deformation-induced stress in the field by the shear and dilation displacement of  $j$ th fracture unit is

$$\begin{aligned}\sigma_{xx}^j &= 2GD_s^j (2\bar{f}_{,\bar{x}\bar{y}} + \bar{y}\bar{f}_{,\bar{x}\bar{y}\bar{y}}) + 2GD_n^j (\bar{f}_{,\bar{y}\bar{y}} + \bar{y}\bar{f}_{,\bar{y}\bar{y}\bar{y}}) \\ \sigma_{yy}^j &= 2GD_s^j (-\bar{y}\bar{f}_{,\bar{x}\bar{y}\bar{y}}) + 2GD_n^j (\bar{f}_{,\bar{y}\bar{y}} - \bar{y}\bar{f}_{,\bar{y}\bar{y}\bar{y}}) \\ \sigma_{xy}^j &= 2GD_s^j (\bar{f}_{,\bar{y}\bar{y}} + \bar{y}\bar{f}_{,\bar{x}\bar{y}\bar{y}}) + 2GD_n^j (-\bar{y}\bar{f}_{,\bar{x}\bar{y}\bar{y}})\end{aligned}\quad (9)$$

where

$$\begin{aligned}f(\bar{x}, \bar{y}) &= -\frac{1}{4\pi(1-\nu)} \left[ \bar{y} \left( \arctan \frac{\bar{y}}{\bar{x}-a} - \arctan \frac{\bar{y}}{\bar{x}+a} \right) \right. \\ &\quad - (\bar{x}-a) \ln \sqrt{(\bar{x}-a)^2 + \bar{y}^2} \\ &\quad \left. + (\bar{x}+a) \ln \sqrt{(\bar{x}+a)^2 + \bar{y}^2} \right]\end{aligned}\quad (10)$$

where the field point  $(x, y)$  must transform to the local  $j$ th fracture unit coordinate  $(\bar{x}, \bar{y})$ . The  $(x_j, y_j)$  is the midpoint of the  $j$ th fracture unit.

$$\begin{aligned}\bar{x} &= (x - x_j) \cos \beta_j + (y - y_j) \sin \beta_j \\ \bar{y} &= -(x - x_j) \sin \beta_j + (y - y_j) \cos \beta_j\end{aligned}\quad (11)$$

The deformation-induced stress is approximated as the sum of the all the displacement fracture unit, as shown in the following:

$$\begin{aligned}\sigma_{xx} &= \sum_{j=1}^n \sigma_{xx}^j \\ \sigma_{yy} &= \sum_{j=1}^n \sigma_{yy}^j \\ \sigma_{xy} &= \sum_{j=1}^n \sigma_{xy}^j\end{aligned}\quad (12)$$

**2.3. Thermal-Induced Aperture and Stress Model.** During the hydroshearing stimulation process, a large heat transfers from the reservoir matrix into the injected cold fluid. The temperature change causes thermal-induced stress and displacement within the rock and fracture. The thermal-induced stress model under the condition of the continuous heat source is deduced by using Green's function [25].

$$\begin{aligned}\bar{\sigma}_{ij}^c(x, y, s) &= -Q\rho_f c_f \int_0^{L_f} s \bar{\sigma}_{ij}^{cs}(R, s) \frac{\partial \bar{T}(x', 0, s)}{\partial x'} dx'\end{aligned}\quad (13)$$

where

$$\begin{aligned}\bar{\sigma}_{rr}^{cs} &= \frac{-E\alpha_T}{4\pi(1-\nu)K_{m,eff}} \frac{1}{s} \left[ \frac{2}{\xi^2} - K_2(\xi) + K_0(\xi) \right] \\ \bar{\sigma}_{\theta\theta}^{cs} &= \frac{-E\alpha_T}{4\pi(1-\nu)K_{m,eff}} \frac{1}{s} \left[ \frac{2}{\xi^2} - K_2(\xi) - K_0(\xi) \right]\end{aligned}\quad (14)$$

$$\xi = R \sqrt{\frac{\rho_m c_m s}{K_{m,eff}}}$$

The displacement of the granite matrix can be given by the following Navier equation [20]:

$$\begin{aligned} G\nabla^2 u_y(x, y, t) + \frac{G}{1-2\nu} \nabla [\nabla \cdot u_y(x, y, t)] \\ = \frac{2G(1+\nu)}{1-2\nu} \alpha_T \nabla T(x, y, t) \end{aligned} \quad (15)$$

where  $G$  is the shear modulus,  $\nu$  is the Poisson's ratio, and  $u_y$  is the displacement of the fracture to the normal direction. Integrating (15) from the fracture surface to infinity, the aperture change of the fracture surface is shown as

$$\begin{aligned} -u_y(x, 0, t) &= \frac{(1+\nu)\alpha_T}{1-\nu} \int_0^\infty \Delta T(x, y, t) dy \\ \Delta T(x, y, t) &= T(x, y, t) - T_\infty \end{aligned} \quad (16)$$

where  $\Delta T$  is the temperature difference. Differentiating (16) with respect to time and using the heat expression for heat conduction in the rock matrix,

$$\begin{aligned} \frac{\partial u_y}{\partial t} &= \frac{1}{2} \frac{\partial w(x, t)}{\partial t} \\ &= \frac{(1+\nu)\alpha_T K_{m,eff}}{(1-\nu)\rho_m c_m} \frac{\partial \Delta T(x, y, t)}{\partial y} \Big|_{y=0} \end{aligned} \quad (17)$$

The Bodvarsson analytical solution [26] was used to avoid the numerical oscillations and uncertainty in numerically calculated heat flux at the interface.

$$\begin{aligned} \frac{T_{m0} - T(x, y, t)}{T_{m0} - T_{in}} \\ = efc \left[ \frac{\sqrt{K_{m,eff}\rho_m c_m}}{Qc_f \rho_f \sqrt{t}} x + \sqrt{\frac{\rho_m c_m}{K_{m,eff} t}} \frac{y}{2} \right] \end{aligned} \quad (18)$$

Assuming that the initial temperature of the granite rock is  $T_{m0}$  and  $T_{in}$  is the injection fluid temperature and  $C_w$  is the water specific heat. Differentiating (18) with respect to  $y$ ,

$$\frac{\partial T(x, y, t)}{\partial y} \Big|_{y=0} = \frac{2\Delta T A_2}{\sqrt{\pi}} \exp[-(A_1)^2] \quad (19)$$

Substitution (19) into (17) yields

$$\begin{aligned} \frac{\partial w(x, t)}{\partial t} \\ = \frac{2(1+\nu)\alpha_T K_{m,eff}}{(1-\nu)\rho_m c_m} \left( \frac{2\Delta T A_2}{\sqrt{\pi}} \exp[-(A_1)^2] \right) \end{aligned} \quad (20)$$

where  $A_1$  and  $A_2$  are

$$\begin{aligned} A_1 &= \frac{x\sqrt{K_{m,eff}\rho_m c_m}}{Q\rho_f c_f \sqrt{t}}, \\ A_2 &= \frac{\sqrt{\rho_m c_m}}{2\sqrt{K_{m,eff} t}} \end{aligned} \quad (21)$$

TABLE 2: Parameters used in numerical calculations.

Parameters	Value
Injected water density (kg/m <sup>3</sup> )	1000
Injected water heat capacity (J/Kg/K)	4180
Hot dry rock fracture roughness	15
Hot dry rock Young's modulus (Pa)	4E10
Hot dry rock Poisson's ratio	0.28
Hot dry rock density (kg/m <sup>3</sup> )	2650
Hot dry rock initial temperature (°C)	200
Hot dry rock specific heat capacity (J/Kg/K)	1070
Hot dry rock thermal conductivity(J/s/m/K)	2.60
Fracture begin shear expansion coefficient	0.3

**2.4. Rock Matrix Stability Model.** The induced stress will be generated through the deformation of single fracture, which will lead to redistribution of the stress state around the rock matrix. As a result, the rock matrix nodes and unconnected natural fractures may fail under the new stress environment, and the underground fracture network of hot rock is formed by the communication between the natural fractures.

Criterion of rock matrix failure is

$$\sigma_1 \geq \sigma_3 + \frac{2(c + \sigma_3 \tan \varphi_b)}{(1 - \tan \varphi_b \cot \alpha) \sin 2\alpha} \quad (22)$$

Criterion of unconnected fracture failure is

$$\sigma_1 \geq \sigma_3 + \frac{2\sigma_3 \tan \varphi_b}{(1 - \tan \varphi_b \cot \alpha) \sin 2\alpha} \quad (23)$$

where  $\sigma_1, \sigma_3$  are maximum and minimum horizontal stress;  $c$  is rock cohesion, MPa;  $\varphi_b$  is basic friction angle;  $\alpha$  is the angle between maximum horizontal stress and effective normal stress.

### 3. Numerical Solution and Verification

**3.1. Model Parameters and Boundary Condition.** The high temperature and fractured granite reservoir system is considered two sets of coupled partial differential equations for the natural fracture and the matrix. All the various input parameters used in the simulations are reported in Table 2.

The problem boundary condition of the fracture is prescribed along with the fracture direction and the rock matrix boundary is specified at the interface of the fracture-matrix. The initial and boundary conditions are (24)~(26) for the rock matrix and the within natural fracture, respectively, are

$$\begin{aligned} T_f(x, 0, 0) &= T_m(x, y, 0) = T_0 \\ w(x, 0, 0) &= w_0 \end{aligned} \quad (24)$$

$$\begin{aligned} P_f(x, 0, 0) &= P_{out} \\ T_f(0, 0, t) &= T_{in} \\ q(0, 0, t) &= q_{in} \end{aligned} \quad (25)$$

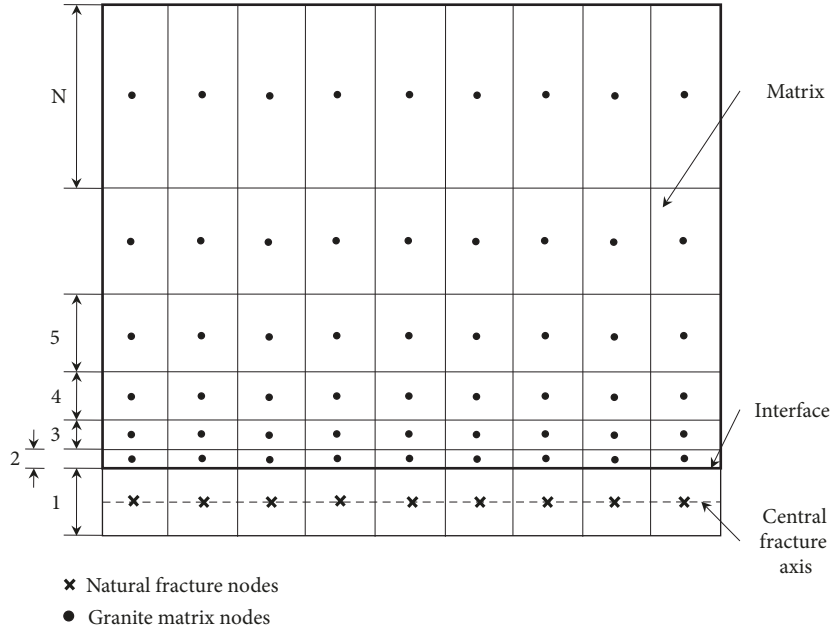


FIGURE 4: Discretization of the solution domain satisfying both the cell-based finite volume and the nodal-based finite-difference schemes [15].

$$\begin{aligned} \left. \frac{\partial T_m}{\partial y} \right|_{(x, L, m, t)} &= 0 \\ \left. \frac{\partial T_m}{\partial x} \right|_{(0, t)} &= \left. \frac{\partial T_m}{\partial x} \right|_{(L, f, t)} = 0 \end{aligned} \quad (26)$$

**3.2. Numerical Solution.** In this study, the system is solved numerically using a second-order central-difference finite-difference scheme. The solution is iterated in each time step to satisfy the continuity at the matrix-fracture interface. The grid size in the fracture is maintained uniform whereas a nonuniform size is adopted in the rock matrix; it is to be noted that all the fracture and matrix grid size does not change with time, shown as in Figure 4.

The heat transfer model is used to calculate the temperature profile through the coupling of the fracture and the matrix. The pressure distribution within the fracture is updated from the thermal-induced aperture change. The fracture deformation due to the effective pressure change will be analyzed through the fracture constitutive model. The coupling between thermal, deformation, and hydroflow is iterated at each time step. The convergence criterion for heat transfer is that the temperature difference is less than 0.01K. The convergence criterion for THM coupling is that the aperture difference is less than 0.00001mm. After the THM coupling, the new stress environment of each matrix nodes is updated from the calculation of induced stress. The stability analysis of matrix nodes is also completed. The coupling between THM, induced stress, and matrix stability is illustrated in Figure 5.

**3.3. Verification.** As previously described in this paper, the shear displacement and dilation behavior of a single fracture are compared with a numerical solution, as shown in Figure 6.

It is to be noted that the prepeak behavior is not elastoplastic and it is simply a nonlinear (prepeak) model. The bottom of the rock is fixed in all three directions and the top displacement will be applied in one of the shear directions. In this comparative analysis, the confining normal stress is 2MPa, the joint's roughness is 15, and the joint's compressive strength is 150MPa, and other data has been shown in Table 2. The results indicate that the lab test and the numerical model agree very well.

During the verification of the heat transfer model, the temperature in both the rock matrix and natural fracture is a relative temperature which is defined as the ratio of current temperature to the initial reservoir temperature. The initial temperature of the matrix is 200°C and the injection water is 20°C. The water velocity between the inlet and outlet is maintained at a constant value of 50 m per day, and the other thermal parameters of the water/matrix are given in Table 2. The simulation results of the heat transfer and thermal-induced aperture for verification are shown in Figures 7 and 8. All comparative studies have shown that the numerical model and other researcher's results are in good agreement.

## 4. Case Study and Matrix Stability Analysis

**4.1. Hydroshearing Stimulation and Pressure Fitting.** RRG-9 ST1 well is located in Cassia County, southwestern Idaho. The open hole section of the well, from 5551 to 5900 ft MD, consists of granite and minor diabase. The tested initial minimum horizontal stress is 22MPa and the maximum is 32MPa [27, 28]. The hydroshearing stimulation target showed evidence of more than eighty natural fractures and the maximum temperature range from 130°C to 150°C. After cementing, a hydroshearing stimulation program was carried out in the open hole section in 2013. The objective of the

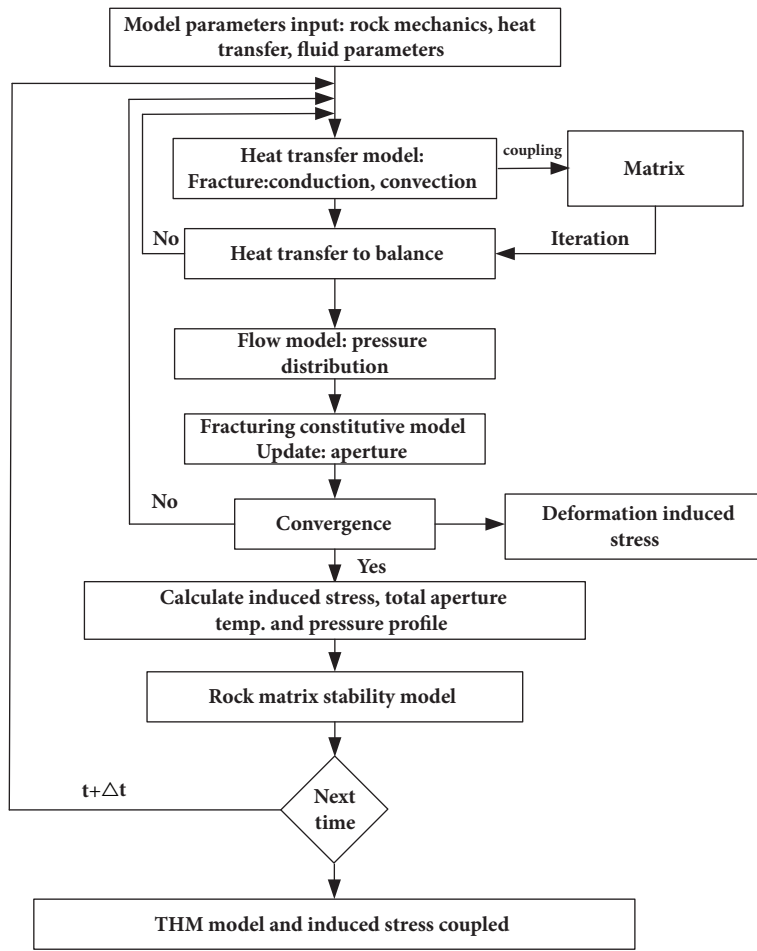


FIGURE 5: Coupled thermal-hydraulic-mechanical model and induced stress.

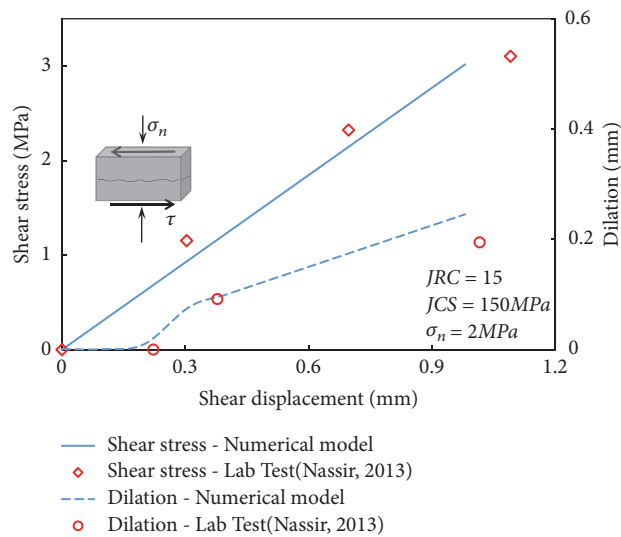


FIGURE 6: Comparison between the lab test and the numerical model for shear stress and displacement.

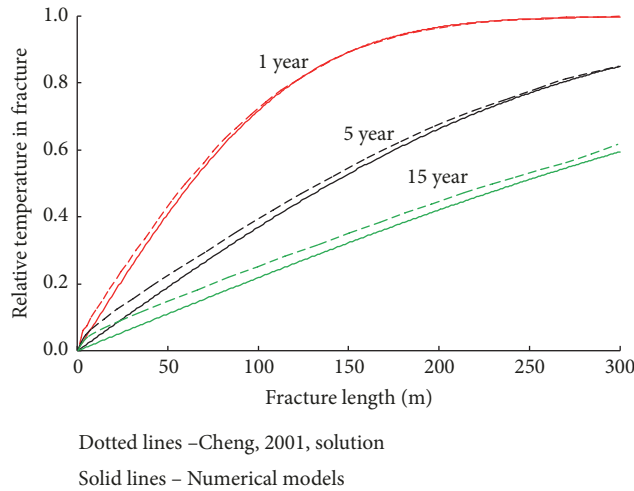


FIGURE 7: Comparison the normalized temperature distribution between numerical model and Cheng's solution in the fracture.

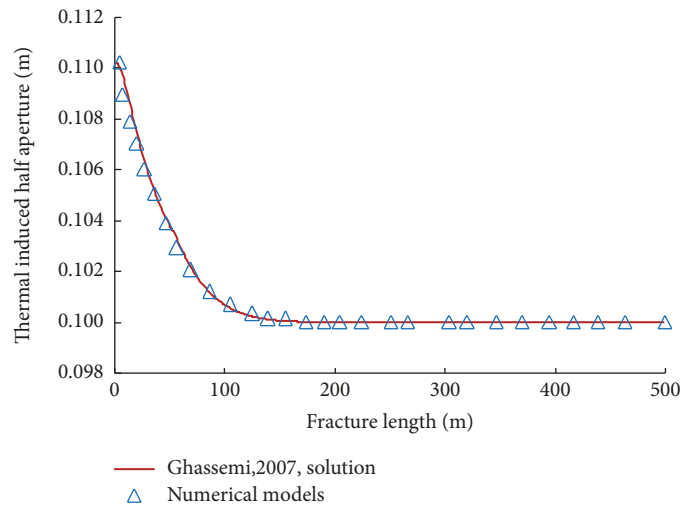


FIGURE 8: Comparison the thermal-induced aperture along the fracture between numerical model and Ghassemi's solution.

fracturing program is to improve the injectivity of the well. The entire stimulation can be divided into three stages: unstable pumping stage, stable pumping stage, and efficient pumping stage. In the unstable pumping stage, the injected water temperature from high (40°C) decreased to low (12°C), as shown in Table 3.

At the beginning of the fracturing, high temperature (40°C) water was injected into the fracture. The permeability of the fracture was very low and nearly equal to the initial conductivity while the surface pumping pressure increases with the injection rate. After unstable pumping stage, the permeability of the natural fracture is greatly improved; the ground injection pressure is maintained at a constant value. The pumping pressure fitting shows that the simulation results are in good agreement with the well site fracturing date, as shown in Figure 9. The coupled THM model to represent fracture aperture change and heat transfer worked well.

4.2. *Fracture Aperture and Temperature Profile.* Having verified the basic coupled fracture-matrix, heat transfer model, and fracture deformation equations, the total aperture change along the fracture is computed. Both models that affect the aperture change have been used in this work and the results are shown in Figure 10. It can be observed that both expressions yield similar trends at different pumping stages. Under the combined influence of thermal stress and decreasing net pressure, the fracture aperture increases with the shearing fracturing time. After 241 days of injection simulation, the change in fracture aperture in RRG-9 ST1 well occurs over a short zone near the injection well (the aperture change zone is about 10m). The fracture aperture is at a maximum (0.03m) near the injection well, and this maximum aperture decreases along the fracture axis as the fluid circulation continues between the inlet and outlet wells.

The combined influence of thermal stress and decrease in net pressure induced deformation in a fracture-matrix coupled system on fracture aperture is illustrated in Figure 11.

TABLE 3: Hydroshearing stimulation schedule of the RRG-9 ST1 well.

Hydro-shearing stimulation	Injected water temperature, °C	Injection rate, m <sup>3</sup> /min	Pumping pressure, Psi	Time, day
Unstable pumping stage	40	0.16-0.53-0.99	270-540-810	35
Stable pumping stage	12	0.96	740-520	6
Efficient pumping stage	29	0.5	270	90
	45	0.8-1.9	260	110

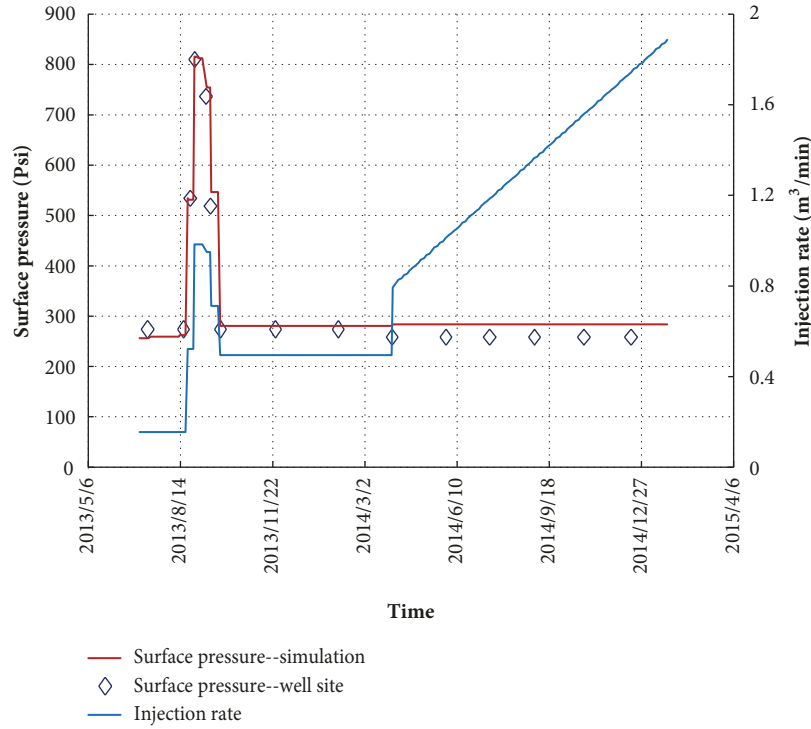


FIGURE 9: Pressure fitting on RRG-9 ST1 well hydroshearing simulation.

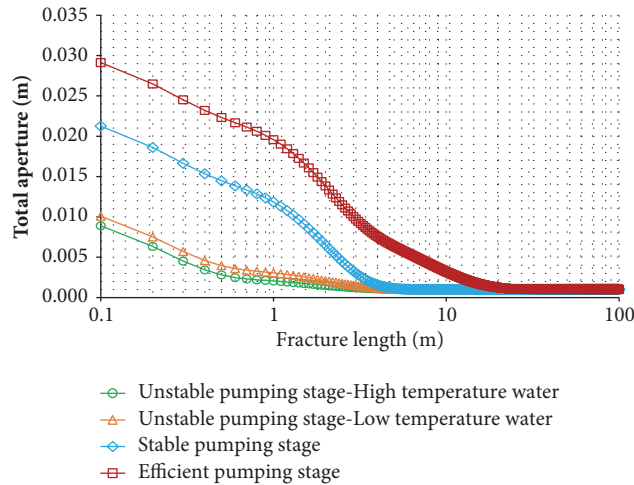


FIGURE 10: Change in fracture total aperture along the fracture due to coupling of thermal and mechanical.

Two distinct regimes in fracture aperture variation can be observed along the fracture between the inlet and outlet wells. The first regime occurs near the injection well, about 10 meters; the contribution of fracture conductivity

is mainly from the thermal-induced aperture. The second regime, away from the injection well, the conductivity of the fracture is dominated by shear dilation. Therefore, the best way to enhance the conductivity of the underground

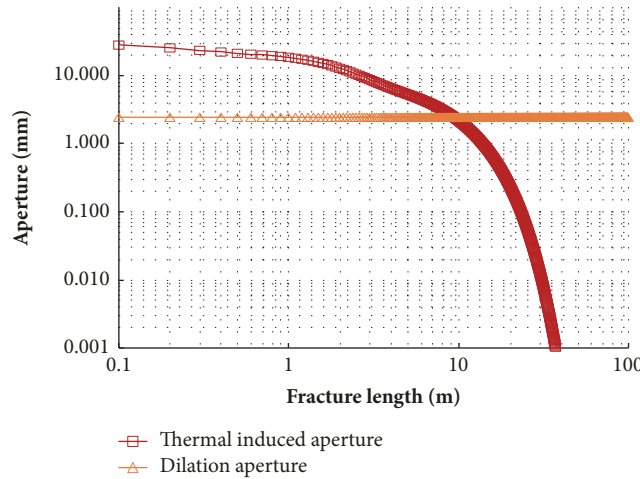


FIGURE 11: Change in thermal-induced aperture and dilation aperture along the fracture.

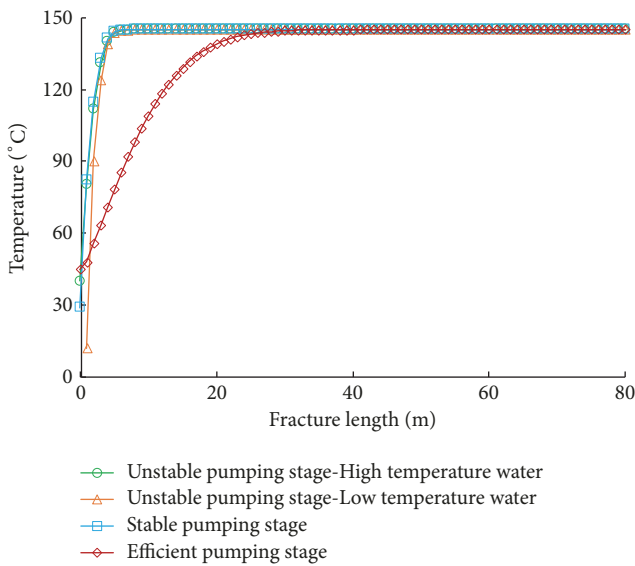


FIGURE 12: Change in temperature profile along the fracture in different pumping stage.

hundreds of meters' fracture area is the using of shear dilation.

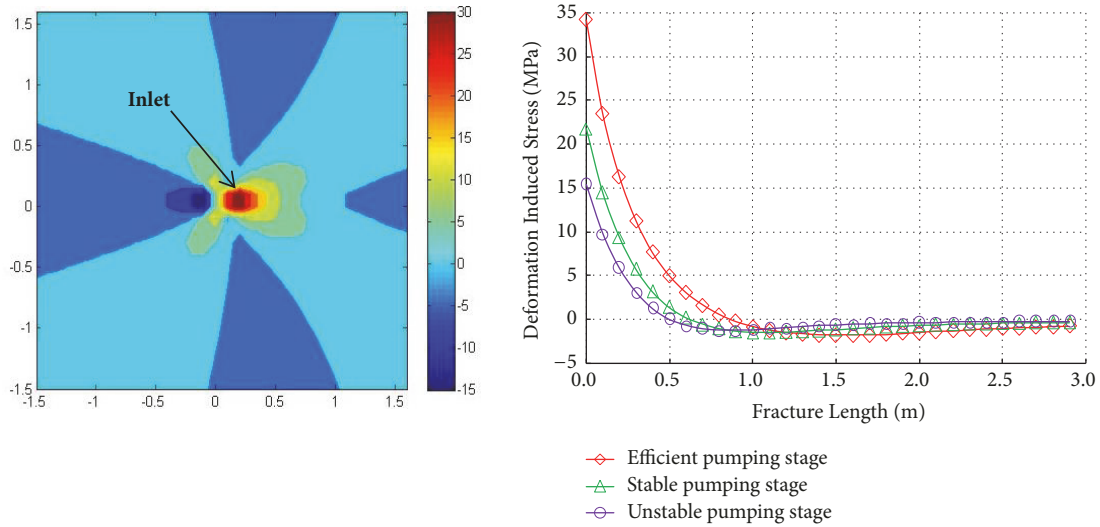
The temperature profiles along the fracture axis after three different pumping stages are illustrated in Figure 12. The plot of the temperature profile is very sharp near the injection area, which indicates a large heat transfer from the reservoir into the fracture fluid. During long-term fracturing, it requires a greater distance from the injection well for the fluid to reach the matrix initial temperature. In this case, after 241 days' injection, the temperature of the circulating fluid nearly reaches the matrix initial temperature at 20 m from the injection well. That is why the thermal-induced aperture change regime is very small. It is indirectly proved that the hot reservoir has a strong thermal energy mining capacity.

4.3. Matrix Stability and Fracture Network Expansion. After the calculation of fracture total aperture and heat transfer

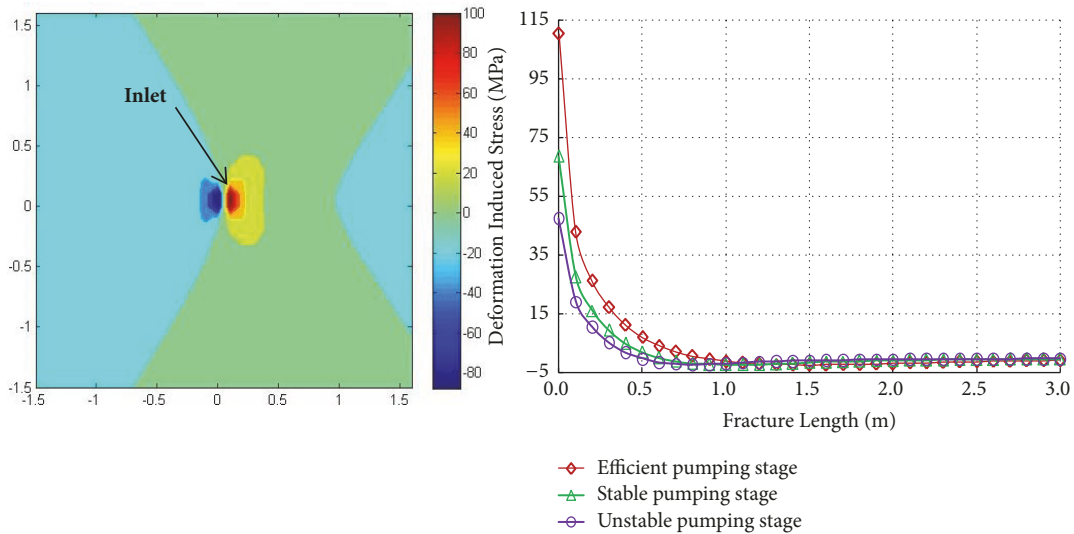
in each time step, the deformation-induced stress and thermal-induced stress are calculated. Figure 13 shows the deformation-induced stress in minimum and maximum horizontal stress direction. The deformation-induced minimum horizontal stress and maximum horizontal stress have a similar change trend and have the maximum positive value at the injection point. In other words, the stress state of the matrix nodes is increased. In this case, after 241 days' injection, the maximum value of the deformation-induced stress in minimum and maximum horizontal stress direction are 35 MPa and 101 MPa, separately. The maximum value quickly reduced to a stable value in a very short range near the injection well (in this case, the affected range is about 1 meter).

The thermal-induced stress in both minimum and maximum horizontal stress directions are negative, which means that tensile stress is formed near the injection area, as shown in Figure 14. In this RRG-9 ST1 well hydroshearing simulation case, after 241 days' injection, the maximum value of the thermal-induced stress in minimum and maximum horizontal stress direction are -3 MPa and -4.5 MPa, separately. The thermal-induced stress affected range is about 2 meters. Therefore, the deformation-induced stress has a large value with a smaller affected range; on the contrary, thermal-induced stress has a small value with a larger affected range.

After the given of induced stress, the new stress state of the matrix's nodes can be updated. The new stress state consists of three parts: initial stress, deformation-induced stress, and thermal-induced stress. The new stress state will affect the stability of the rock matrix. In other words, when the new stress state of the matrix nodes is located above the strength envelope, the stability of the matrix node will be destroyed. Figure 15 shows the relationship between the new stress state and the strength envelope of the matrix (left), the failure modes, and their position in different pumping stages (right). In this simulation case, after three-stage fracturing, seven matrix nodes are located above the strength envelope. With the increase in fracturing pump time, the number of the failure nodes and the affected range also



(a) Minimum horizontal stress direction



(b) Maximum horizontal stress direction

FIGURE 13: The variation of deformation-induced stress in minimum and maximum horizontal stress direction in different pumping stages.

increase. This mechanism is helpful to create complex fracture networks.

### 5. Conclusions

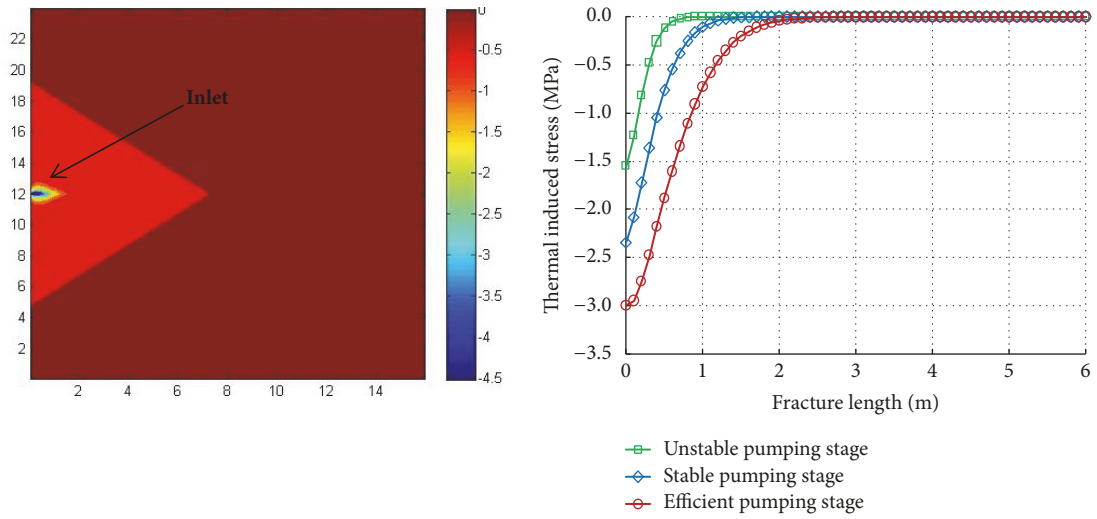
A coupled THM model is developed to simulate the combined effect of fracture fluid flow, heat transfer from the matrix to injected fluid, and shearing dilation behaviors in a coupled fracture-matrix hot volcanic reservoir system. In view of the expansion of the fracture network, deformation and thermal-induced stress models are added to the matrix nodes in situ stress environment in each time step to analyze the stability of the matrix.

The coupled THM modeling results indicate that, in these case conditions, the change in fracture aperture due to thermoelastic stress occurs near the injection well, thus increasing the fracture opening and playing a dominant role.

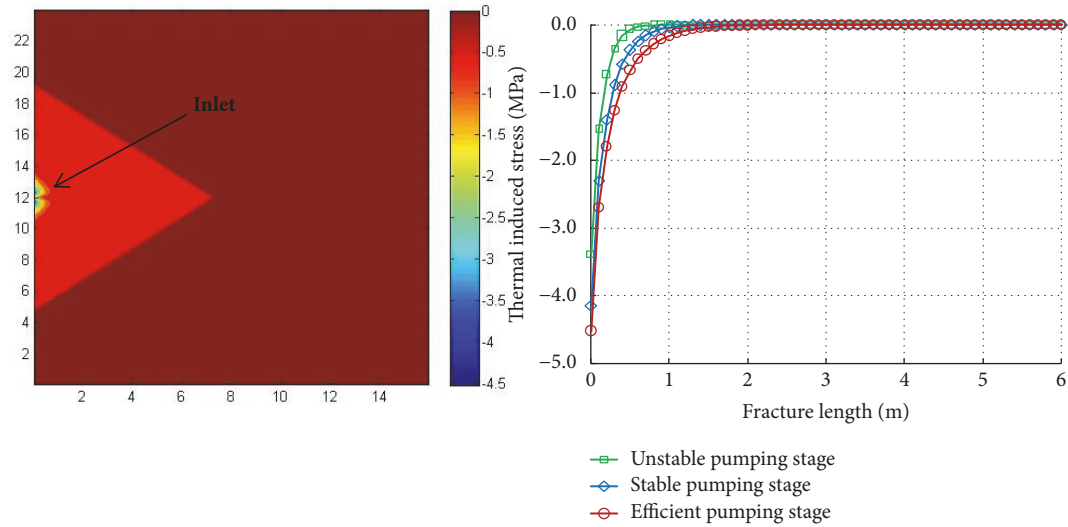
Away from the injection well, the conductivity of the fracture is contributed by shear dilation. Therefore, the best way to enhance the conductivity of the underground hundreds of meters' fracture area is the using of shear dilation.

The induced stress simulation results indicate that deformation-induced stress is a compressive stress with a positive and thermal-induced stress is tensile stress with a negative value. The induced stress has the maximum value at the injection point; the deformation-induced stress has a large value with smaller affected range; on the contrary, thermal-induced stress has a small value with larger affected range.

The new stress state of the matrix nodes is updated by initial stress, deformation-induced stress, and thermal-induced stress. The matrix stability simulation results indicate, in this case, some matrix nodes are located above the strength envelope after hydroshearing stimulation, which means the



(a) Minimum horizontal stress direction



(b) Maximum horizontal stress direction

FIGURE 14: The variation of thermal-induced stress in minimum and maximum horizontal stress direction in different pumping stage.

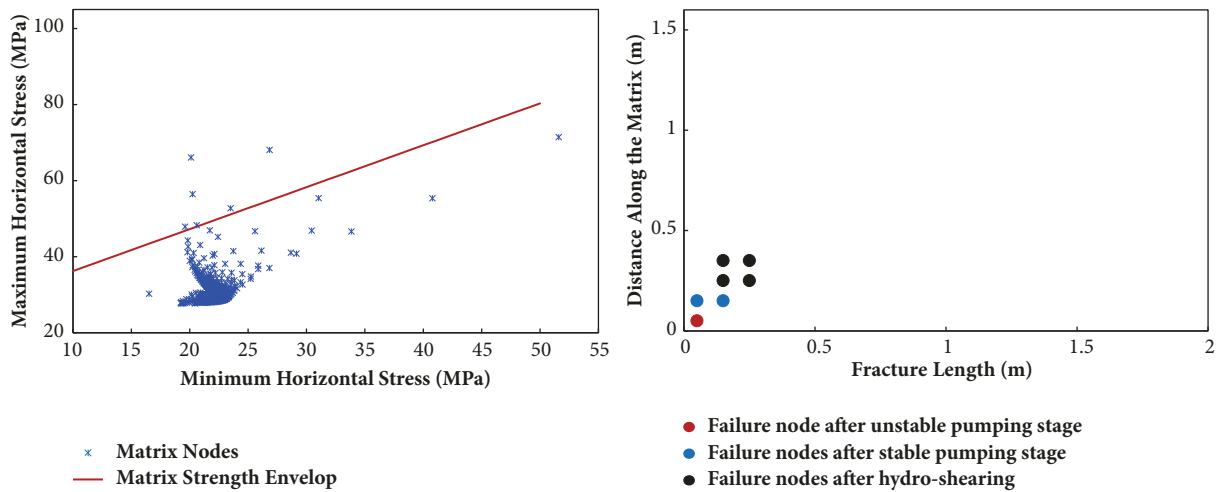


FIGURE 15: The relationship between the new stress state and the strength envelope of the matrix (left), the failure modes, and their position in different pumping stages (right).

stability of the matrix node will be destroyed. This mechanism is helpful to create complex fracture networks.

### Data Availability

The data used to support the findings of this study are available from the corresponding author upon request.

### Conflicts of Interest

The authors declare that they have no conflicts of interest.

### Acknowledgments

The authors would like to acknowledge the support of the National Science Fund for Distinguished Young Scholars (ID: 51525404) and Foundation of China Scholarship Council (File no. 201608510077).

### References

- [1] Z. Feng, J. Liu, P. Wang, S. Chen, and Y. Tong, "oil and gas exploration field: volcanic hydrocarbon reservoirs-Enlightenment from the discovery of the large gas field in Songliao basin," *Diqiu Wuli Xuebao*, vol. 54, no. 2, pp. 269–279, 2011.
- [2] S. A. Holditch, "The Increasing Role of Unconventional Reservoirs in the Future of the Oil and Gas Business," *Journal of Petroleum Technology*, vol. 55, no. 11, pp. 34–79, 2003.
- [3] Z.-Q. Feng, "Volcanic rocks as prolific gas reservoir: A case study from the Qingshen gas field in the Songliao Basin, NE China," *Marine and Petroleum Geology*, vol. 25, no. 4-5, pp. 416–432, 2008.
- [4] J. Guo, B. Luo, C. Lu, J. Lai, and J. Ren, "Numerical investigation of hydraulic fracture propagation in a layered reservoir using the cohesive zone method," *Engineering Fracture Mechanics*, vol. 186, pp. 195–207, 2017.
- [5] J. Guo, J. Wang, Y. Liu, Z. Chen, and H. Zhu, "Analytical analysis of fracture conductivity for sparse distribution of proppant packs," *Journal of Geophysics and Engineering*, vol. 14, no. 3, pp. 599–610, 2017.
- [6] Y. Xiao, G. Jianchuan, and J. McLennan, "Deformation and initiation in Fracture Due To Hydro-Shearing and Induced Stress in Enhanced Geothermal System," in *Paper presented at the 4th ISRM Young Scholars Symposium on Rock Mechanics*, 2017.
- [7] Y. Xiao, G. Jianchuan, and B. Luo, "Characterization of Fracture Conductivity of Hydraulic Fracturing in Hot Dry Rock Exploitation," in *Paper presented at the 51st U.S. Rock Mechanics/ Geomechanics Symposium*, 2017.
- [8] D. Vogler, F. Amann, P. Bayer, and D. Elsworth, "Permeability Evolution in Natural Fractures Subject to Cyclic Loading and Gouge Formation," *Rock Mechanics and Rock Engineering*, vol. 49, no. 9, pp. 3463–3479, 2016.
- [9] A. P. Rinaldi, J. Rutqvist, E. L. Sonnenthal, and T. T. Cladouhos, "Coupled THM Modeling of Hydroshearing Stimulation in Tight Fractured Volcanic Rock," *Transport in Porous Media*, vol. 108, no. 1, pp. 131–150, 2015.
- [10] J. Taron and D. Elsworth, "Thermal-hydrologic-mechanical-chemical processes in the evolution of engineered geothermal reservoirs," *International Journal of Rock Mechanics and Mining Sciences*, vol. 46, no. 5, pp. 855–864, 2009.
- [11] J. Rutqvist, Y.-S. Wu, C.-F. Tsang, and G. Bodvarsson, "A modeling approach for analysis of coupled multiphase fluid flow, heat transfer, and deformation in fractured porous rock," *International Journal of Rock Mechanics and Mining Sciences*, vol. 39, no. 4, pp. 429–442, 2002.
- [12] J. Taron, D. Elsworth, and K.-B. Min, "Numerical simulation of thermal-hydrologic-mechanical-chemical processes in deformable, fractured porous media," *International Journal of Rock Mechanics and Mining Sciences*, vol. 46, no. 5, pp. 842–854, 2009.
- [13] Q. Gan and D. Elsworth, "Production optimization in fractured geothermal reservoirs by coupled discrete fracture network modeling," *Geothermics*, vol. 62, pp. 131–142, 2016.
- [14] G. Izadi and D. Elsworth, "The influence of thermal-hydraulic-mechanical- and chemical effects on the evolution of permeability, seismicity and heat production in geothermal reservoirs," *Geothermics*, vol. 53, pp. 385–395, 2015.
- [15] G. S. Kumar and A. Ghassemi, "Numerical modeling of non-isothermal quartz dissolution/precipitation in a coupled fracture-matrix system," *Geothermics*, vol. 34, no. 4, pp. 411–439, 2005.
- [16] P. Olasolo, M. C. Juárez, M. P. Morales, S. Damico, and I. A. Liarte, "Enhanced geothermal systems (EGS): A review," *Renewable & Sustainable Energy Reviews*, vol. 56, pp. 133–144, 2015.
- [17] S. L. Crouch, A. M. Starfield, and F. J. Rizzo, "Boundary element methods in solid mechanics," *Journal of Applied Mechanics*, vol. 50, p. 704, 1983.
- [18] Y. Cheng, "Boundary element analysis of the stress distribution around multiple fractures: Implications for the spacing of perforation clusters of hydraulically fractured horizontal wells," in *Proceedings of the SPE Eastern Regional Meeting 2009: Limitless Potential / Formidable Challenges*, pp. 267–281, USA, September 2009.
- [19] Q. Tao, *Numerical modeling of fracture permeability change in naturally fractured reservoirs using a fully coupled displacement discontinuity method*, Texas AM University, 2010.
- [20] A. Ghassemi and G. Suresh Kumar, "Changes in fracture aperture and fluid pressure due to thermal stress and silica dissolution/precipitation induced by heat extraction from subsurface rocks," *Geothermics*, vol. 360, no. 2, pp. 115–140, 2007.
- [21] E. Barbier, "Geothermal energy technology and current status: An overview," *Renewable & Sustainable Energy Reviews*, vol. 6, no. 1-2, pp. 3–65, 2002.
- [22] J. Bradford, J. Moore, M. Ohren, J. McLennan, W. L. Osborn, and E. Majer, "Recent Thermal and Hydraulic Stimulation Results at Raft River," in *ID EGS Site*, Paper presented at the Fourtieth Workshop on Geothermal Reservoir Engineering, Stanford University, Stanford, California, 2015.
- [23] N. Barton, S. Bandis, and K. Bakhtar, "Strength, deformation and conductivity coupling of rock joints," in *Proceedings of the Paper presented at the International Journal of Rock Mechanics and Mining Sciences & Geomechanics Abstracts*, 1985.
- [24] N. Barton and V. Choubey, *The shear strength of rock joints in theory and practice*, Rock Mechanics and Rock Engineering, 1977.
- [25] S. Tarasovs and A. Ghassemi, "Propagation of a system of cracks under thermal stress," in *Proceedings of the 45th US Rock Mechanics / Geomechanics Symposium*, USA, June 2011.

- [26] G. Bodvarsson, "On the temperature of water flowing through fractures," *Journal of Geophysical Research*, vol. 74, no. 8, pp. 1987–1992, 1969.
- [27] J. Bradford, J. McLennan, J. Moore, D. Glasby, D. Waters, and R. Kruwell, "Recent developments at the Raft River geothermal field," in *Proceedings of the Paper presented at the Proceedings*, Stanford University, Stanford, California, 2013.
- [28] C. Jones, J. Moore, W. Teplow, and S. Craig, "Geology and hydrothermal alteration of the Raft River geothermal system," in *Proceedings of the Idaho. Paper presented at the Proceedings, Thirty-Sixth Workshop on Geothermal Reservoir Engineering*, Stanford University, Stanford, California, 2011.



**Hindawi**

Submit your manuscripts at  
[www.hindawi.com](http://www.hindawi.com)

